

Published in *Neuroimage*, Volume 49, Issue 4, pp 2958-2965, 2010.

The original publication is available at www.sciencedirect.com via the following DOI: <http://dx.doi.org/10.1016/j.neuroimage.2009.11.027>

Diffusion Tensor Imaging Segments the Human Amygdala In Vivo

Eugenia Solano-Castiella, Alfred Anwander, Gabriele Lohmann, Marcel Weiss, Carol Docherty, Stefan Geyer, Enrico Reimer, Angela D. Friederici, and Robert Turner

Max Planck Institute for Human Cognitive and Brain Sciences, Stephanstrasse 1a, 04103
Leipzig, Germany

Corresponding Author. Professor Robert Turner. Max Planck Institute for Human Cognitive and Brain Sciences, Department of Neurophysics, Stephanstrasse 1a, 04103 Leipzig, Germany. Tel: +49-341-9940-2242. Fax: +49-341-9940-2448

<http://www.cbs.mpg.de>

Preprint submitted to NeuroImage

Final draft: 14th October 2009

Abstract

The amygdala plays an important role in emotion, learning, and memory. It would be highly advantageous to understand more precisely its internal structure and connectivity, for individual human subjects in vivo. Earlier cytoarchitectural research in post-mortem human and animal brains has revealed multiple subdivisions and connectivity patterns, probably related to different functions. With standard magnetic resonance imaging (MRI) techniques, however, the amygdala appears as an undifferentiated area of grey matter. Using high quality diffusion tensor imaging (DTI) at 3 Tesla, we show diffusion anisotropy in this grey matter area. Such data allowed us to subdivide the amygdala for the first time in vivo. In 15 living subjects, we applied a spectral clustering algorithm to the principal diffusion direction in each amygdala voxel and found a consistent subdivision of the amygdala into a medial and a lateral region. The topography of these regions is in good agreement with the fibre architecture visible in myelin-stained sections through the amygdala of a human post-mortem brain. From these in vivo results we derived a probabilistic map of amygdalar fibre orientations. This segmentation technique has important implications for functional studies in the processing of emotions, cognitive function, and psychiatric disorders and in studying morphometry and volumetry of amygdala subdivisions.

Introduction

The amygdala is a large grey matter complex in the dorsomedial sector of the temporal lobe, where it forms part of the rostromedial and rostradorsal walls of the temporal horn of the lateral ventricle. Experimental findings from laboratory animals and clinical data from humans show that the amygdala plays a key role in emotion, motivation, learning, and memory (Aggleton, 1992). The amygdaloid complex determines the emotional, motivational, and social significance of complex sensory inputs and initiates appropriate neuroendocrine, autonomic, and behavioural responses (Nieuwenhuys et al. 2008; Schirmer et al. 2008). This considerable functional diversity is also reflected on a structural basis. Initially parcellated into more than 30 different cyto- and myeloarchitectonic entities (Brockhaus 1938), there is now widespread agreement that the amygdaloid complex is subdivided into three groups of nuclei (in medio-lateral orientation): (1) the corticomedial group with the cortical and medial nuclei, (2) the central nucleus, and (3) the basolateral group with the accessory basal, basal, and lateral nuclei (Amaral et al. 1992; McDonald 1992; de Olmos 2004; Mai et al. 2008; Nieuwenhuys et al. 2008). These subdivisions are specific elements of various distinct input-output loops. The basolateral group receives visual, auditory, somatosensory, and gustatory inputs, whereas olfactory afferents are mainly restricted to the cortical nucleus. Via the extensive intrinsic connections within the amygdaloid complex (running preferentially in a basolateral-to-dorsomedial direction), these sensory stimuli reach the central and medial nuclei. The extended amygdala (central and medial nuclei, bed nucleus of the stria terminalis, and substantia innominata; cf. Alheid and Heimer 1988) is the main output channel of the amygdaloid complex and projects to many hypothalamic and brain stem areas thus generating endocrine, autonomic, and somatomotor aspects of emotional and motivational states (Heimer et al. 1997; Nieuwenhuys et al. 2008).

Considering the ever-increasing spatial resolution of functional imaging studies, it would be a challenge to disentangle the specific functions of the individual amygdaloid nuclei, as suggested by the input-output loops described above. Unfortunately, with standard magnetic resonance imaging (MRI) sequences, the amygdala appears as a relatively uniform grey matter region. The individual nuclei can only be delineated by differences in their microanatomical properties (cytoarchitectonics, fibrearchitectonics, chemoarchitectonics; cf. de Olmos 2004) which are still beyond the spatial resolution of MRI.

One way to overcome this dilemma is the generation of cytoarchitectonic probabilistic maps in standard anatomical space. Specific amygdaloid nuclear groups are defined cytoarchitectonically in cell-stained whole brain sections. Their topography is then reconstructed in 3-D and warped to the reference space of the Montreal Neurological Institute (MNI) single subject brain. Superimposing the normalized data from ten brains generates a probabilistic map, i.e., a probabilistic description of the spatial variability of each nuclear group in standard MNI space (Amunts et al. 2005). In this format, the maps can then be matched with co-registered functional imaging data (probabilistic microstructural-functional correlation). However, due to the small size of each nuclear group, their close spatial proximity within the amygdala, and inter-individual variability among the ten brains, the population maps overlap to a considerable degree. Only after extensive thresholding (i.e., considering only those voxels of each population map in which four or more out of the ten brains overlap) – and thus discarding of structural information – is it possible to unequivocally assign a given voxel in standard space to a particular population map (Amunts et al. 2005). Furthermore, the invasive and irreversible nature of conventional anatomical studies virtually precludes microstructure and function to be studied in the same brains – such correlations can only be probabilistic in nature.

A new impetus towards mapping microstructure and function in identical brains has come from diffusion tensor imaging (DTI). Providing information about the magnitude and direction of the diffusion of water molecules in the brain and using the orientation of the principal axis of the diffusion tensor (commonly taken as the underlying main fibre direction), this technique has widely been used to map fibre tracts in the white matter both in health and disease (for recent reviews and/or atlases see, e.g., Jellison et al. 2004; Wakana et al. 2004; Mori et al. 2005; Nucifora et al. 2007; Lawes et al. 2008; Assaf and Pasternak 2008; Mori et al. 2008; Van Hecke et al. 2008; Oishi et al. 2008). Finding internal structures within the grey matter is a more challenging task due to its poor directional diffusion properties (i.e., low anisotropy; cf. Jaermann et al. 2008). Higher magnetic field strengths and sophisticated clustering algorithms, however, have, in recent years, set the stage for reproducible and anatomically valid parcellations of the grey matter of the cerebral cortex (Johansen-Berg et al. 2004; Klein et al. 2007; Anwender et al. 2007; Tomassini et al. 2007; Beckmann et al. 2009) and subcortical nuclei, such as the thalamus (Wiegell et al. 2003; Behrens et al. 2003; Johansen-Berg et al. 2005; Devlin et al. 2006) and, more recently, the basal ganglia (Draganski et al. 2008). The amygdala has not been studied so far.

The structural and functional diversity of the amygdaloid complex has prompted us to attempt a DTI-based mapping study of this nuclear region. Specifically we wanted to find out whether the amygdala can be parcellated into subregions which (1) are reproducible across subjects and (2) represent anatomically meaningful entities. If successful, this should be another step forward towards correlating microstructure and function in the same brain.

Materials and Methods

Data Acquisition

We used data from 15 healthy subjects (7 females and 8 males between the ages of 22- 35 years) selected at random from our large in-house MRI database. Subjects were given

diffusion-weighted MRI (Turner et al. 1991) and T1-weighted structural scanning on a whole-body 3 Tesla Trio scanner (Siemens, Erlangen, Germany) equipped with an 8-channel head array coil.

Written informed consent was obtained from all participants in accordance with ethical approval from the University of Leipzig. The T1-weighted structural scans were used for skull-stripping, and the brain images were then co-registered into Talairach space (Talairach and Tournoux 1988). Diffusion-weighted images (DWI) were acquired with a twice-refocused spin-echo echo-planar imaging sequence (TE = 100 ms, TR = 12 s, 128 x 128 image matrix, FOV = 220 x 220 mm²) providing 60 diffusion-encoding gradient directions with a b-value of 1000 s/mm² (Reese et al. 2003; Weiskopf et al. 2007). Seven images without any diffusion weighting (b-value = 0) were obtained at the beginning of the scanning sequence and again after each block of 10 diffusion-weighted images as an anatomical reference for offline motion correction. The interleaved measurement of 72 axial slices with 1.7 mm thickness (no gap) covered the entire brain. Each DWI scan took 13 minutes. Random noise in the data was reduced by averaging 3 acquisitions, resulting in an total acquisition time of a 42 minutes. Cardiac gating was not utilized, in order to limit the acquisition time. Additionally, fat saturation was employed, together with 6/8 partial Fourier imaging, Hanning window filtering, and parallel generalized autocalibrating partially parallel acquisition (GRAPPA, reduction factor = 2).

The 21 images without diffusion weighting distributed in the whole sequence were used to estimate motion correction parameters using rigid-body transformations (Jenkinson et al. 2002), implemented in FSL (FMRIB Software Library, University of Oxford, 2006, <http://www.fmrib.ox.ac.uk/fsl>). Motion correction for the 180 diffusion-weighted images was combined with a global registration to the T1 anatomy computed with the same method. The gradient direction for each volume was corrected using the rotation parameters. The registered

images were interpolated to the new reference frame with an isotropic voxel resolution of 1 mm and the three corresponding acquisitions and gradient directions were averaged. A diffusion tensor and the fractional anisotropy (FA) were computed from the DWI data of each voxel.

Amygdala Segmentation

Automatic segmentation tools, while under active development in several laboratories, are still not fully reliable. The amygdaloid complex is a subcortical structure located deep within the temporal lobe, and several of its boundaries are subtly defined in MR images. We decided to use a more robust manual delineation of the amygdala (Horinek et al. 2007) to exclude extraneous tissue, as far as possible. Individual masks were created for each brain, guided by the 2 mm thick anatomical sections of human cadaver brains shown in the Duvernoy (1999) atlas. The resulting masks were conservatively small.

Coronal limits were defined from rostral to caudal sections by the gyrus ambiens, lateral ventricle, entorhinal area, semilunar gyrus, anterior perforated substance, and hippocampal formation. The sagittal boundaries were defined, from lateral to medial, by the peduncle of the lentiform nucleus, hippocampus, anterior commissure, temporal gyrus, and optic tract. Finally, boundaries in axial sections from ventral to dorsal were defined by the hippocampus, parahippocampal gyrus, piriform lobe, entorhinal area, gyrus ambiens, temporal horn of the lateral ventricle, and semilunar gyrus.

Amygdala Parcellation

All 15 anatomical and DWI data sets were subsequently nonlinearly aligned (Thirion 1998) with a single subject template brain, based on the FA contrast of all images, so that the amygdala regions were located in approximately the same position in all transformed data sets. The masks were transformed likewise. We then computed an intersection across all masks so that a single mask resulted which was common to all data sets.

For each voxel, a diffusion tensor was fitted to the spatially normalized DWI data. This tensor characterizes the water mobility for each voxel (Basser 1993). The preferential fibre direction in each voxel is characterized by the principal eigenvector of the diffusion tensor. The angular direction of the diffusion tensors can be conveniently visualized using an RGB colour coding, so that a specific colour represents a particular fibre orientation (Douek et al. 1991).

To group voxels with comparable tissue orientation within the mask of the amygdala, the similarities between two voxels were computed as the cosine of the angle between the principal diffusion directions. For each hemisphere in each of the 15 data sets, we obtained a similarity matrix in which entries s_{ij} represented the similarity of orientations in voxels i and j . The second and third eigenvector of the diffusion tensor were not used due to the higher noise level in these components related to the low anisotropy in the amygdala which is below 0.2.

Spectral Clustering

We averaged the similarity matrices across all subjects and applied spectral clustering to it (Ng et al. 2002). In order to avoid an arbitrary choice of the number of clusters, we used cross-validations to determine the number of clusters which yielded optimal consistency across subjects and hence the optimal number of clusters. Specifically, we employed a leave-one-out method where each subject's data is left out from the averaging. For each subject, we checked the consistency between the clustering results of the single subject and the average across the remaining subjects. We used Cramer's V for this purpose (Cramer, 1946). It is a widely used measure of nominal association based on chi-square and normalized for table size. It has values in the interval $[0,1]$ where high values indicate good consistency with a value of '1' indicating a perfect match. The inter-subject consistency check was performed for $k = 2, 3, 4, 5$ clusters. The results are listed in Table 1. The most consistent result was found for $k = 2$ in both hemispheres.

	k = 2	k = 3	k = 3	k = 5
Left hemisphere	0.72 ± 0.026	0.58 ± 0.019	0.49 ± 0.012	0.47 ± 0.009
Right hemisphere	0.73 ± 0.034	0.57 ± 0.008	0.52 ± 0.011	0.50 ± 0.011

Table 1. Inter-subject consistency for different numbers of clusters using Cramer's V. The numbers shown are averages across subjects with standard errors.

In order to further check whether a clear separation between at least two clusters exists we applied spectral re-ordering to the averaged similarity matrix. This ordering is obtained via the so-called Fiedler vector which corresponds to the second smallest eigenvector of the graph Laplacian of the similarity matrix (Higham et al. 2007).

In order to study the inter-subject variability, the spectral clustering was applied separately to all subjects. The non-normalized DTI data of the individual amygdala segmentation was separated into two clusters for each hemisphere. The individual results were transformed to the template brain. By voxel-wise counting the number of times each subregion was found, a probability map of the clustering result was created.

Myeloarchitectonic comparison

In order to understand the effect of myelinated tissue within the amygdala on the DTI images, we included in this study histological data from one intact human cadaver brain. The post-mortem period before staining was less than one month.

The specimen was preserved in formalin. Blocks containing the amygdalae were sliced with a thickness of 30 µm. The sections were stained for myelin using the Gallyas (1979) technique. This approach is highly specific for myelin and can render thin fibres visible.

Results

Anisotropy in a Grey Matter Region

The initial somewhat surprising finding was a significant anisotropy in grey matter. Figure 1 shows examples of the general appearance of the amygdala in MR images. Neither the T1-weighted image (A) nor the FA map (B) show definable internal structure, consistent with the relatively low myelin content of this area. However, when images were colour-coded for the main diffusion direction in each voxel, a high degree of organization into compact subregions was revealed (C, D). Groups of amygdalar voxels show characteristically different orientations of the diffusion tensors with relatively sharp boundaries (Fig. 1). The red colour component corresponds to medio-lateral orientation, green labels anterior-posterior, and blue a dorso-ventral dominance.

The myelin stained sections revealed relatively few fibre bundles, visible as darker features, within the regions generally accepted as the amygdaloid nuclei, but at the boundaries (septa) of the nuclei a higher fibre concentration can sometimes be seen. The fibre directions within these septa vary across the amygdala, in accordance with the DTI data. Medially, a band of fibres extends in a roughly lateral-to-medial direction, separating the medial amygdaloid nuclei from the others, and consistent with the more medial of the two DTI clusters found. More laterally, a nearly vertical band of fibres extends through the amygdala from its dorsal surface to the ventral temporal lobe white matter, separating the lateral nuclei from the others, and possibly accounting for the dorso-ventral orientation found by DTI here (Fig. 2).

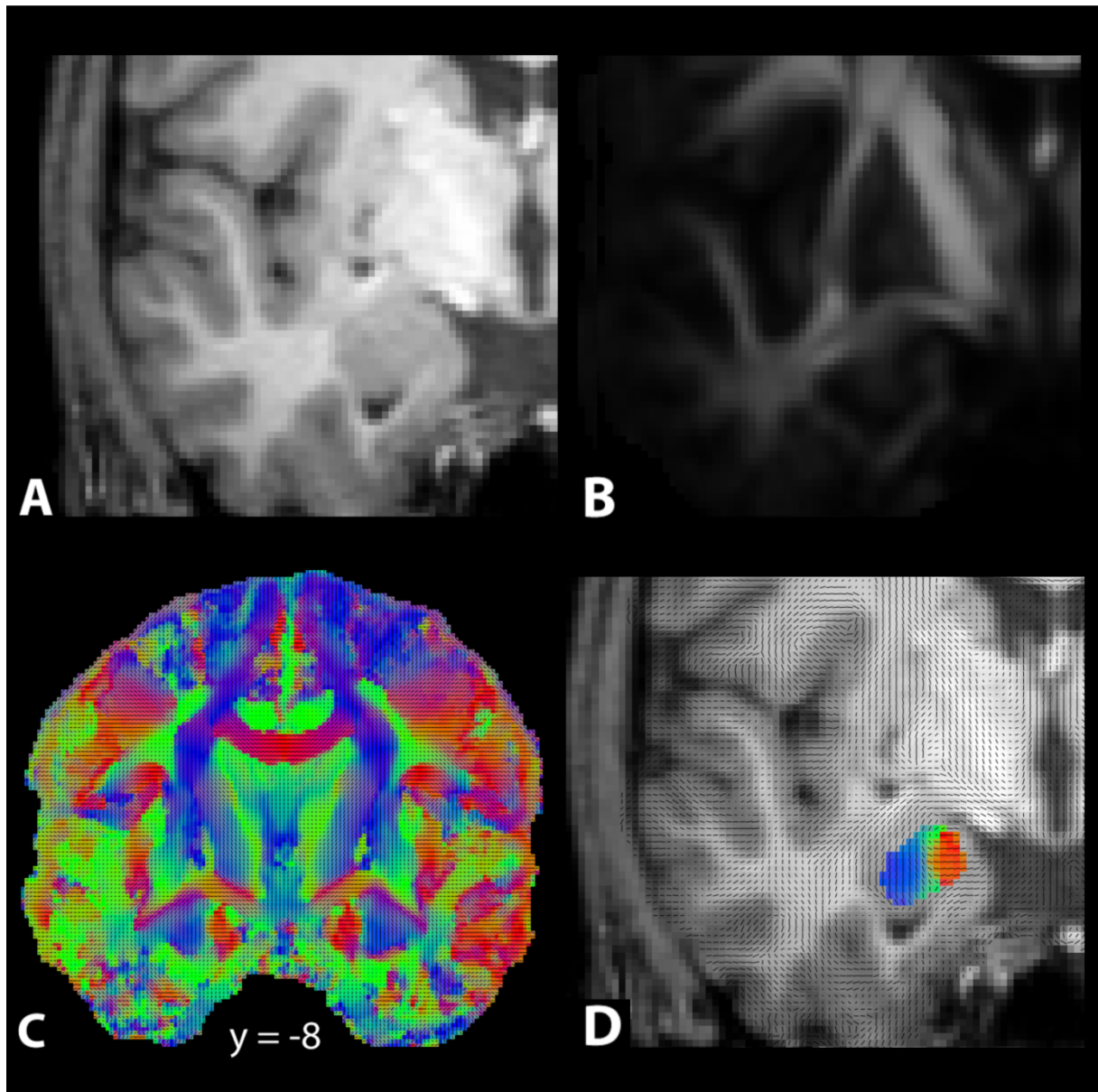


Figure 1. Diffusion data. Coronal MR sections of a single human subject. A, B, D. Enlarged view of the left temporal lobe.. A. T1-weighted structural image. B. Fractional anisotropy (FA) map derived from the diffusion weighted data. C. Diffusion orientation map from the group mean DTI data. Red colour corresponds to medio-lateral direction, green to anterior-posterior, and blue to dorso-ventral orientation. D. Averaged orientation map superimposed on the anatomy of a single subject (amygdala is colour-coded). In C and D the data reveal 3 compact groups of differently oriented voxels not identifiable in panel A and B. Coordinates are in Talairach space.



Figure 2. Myelin-stained coronal section (30 μm thick) of a human post-mortem brain. This shows relatively low myelin content in the amygdaloid complex, with markedly higher fibre density at some boundaries (septa) between the nuclei. The fibre orientations shown in this section may underlie some features of the DTI dataset. In order to indicate the effect of partial voluming, the box represents the size (1.7 mm) of the MRI voxel.

Clusters Found

The mean similarity matrix uses the orientation of the principal eigenvector for every voxel averaged across all 15 data sets after normalization. Using Fiedler vector analysis, this matrix is re-ordered by minimizing the angular differences between adjacent feature vectors. This formalism can provide information regarding the number of clusters that gives maximum reliability. Figure 3 reflects this re-ordering. Note that at least two clearly defined regions are visible along the diagonal of the re-ordered matrix. These areas represent many voxels characterized by similar orientations. A third cluster may possibly reside between the two major compartments but is not clearly discernible.

In the search for robust clusters, the spectral clustering was strongly tested. The most coherent and reproducible number clustering result for both hemispheres was achieved by a

subdivision into two groups of voxels. The left and the right amygdalae were subdivided into compact lateral and medial regions as revealed in Figure 4. The number of clusters was determined by the values of Cramer's V. For two clusters this had an average of 0.73 ± 0.03 , whereas for 3 clusters V was decreased to 0.58 ± 0.01 . The inter-subject variability is included in this analysis.

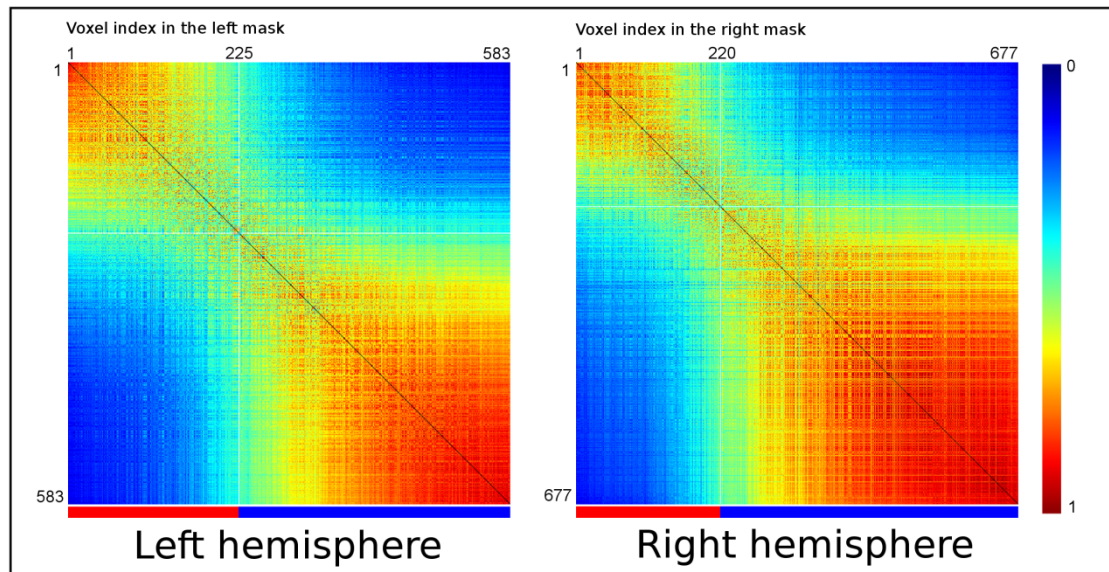


Figure 3. Averaged similarity matrix for diffusion orientation for each hemisphere. The matrix represents the similarity between all pairs of voxels within the amygdala (Left = 583 voxels, Right = 677 voxels). Each voxel is characterized with a main orientation. Spectral re-ordering minimizes the angular distances between feature vectors, providing regions categorized by a particular direction. A perfect orientation match is one. Parallel orientations are labeled in red while orthogonal directions are blue following the displayed colour map. Projection of the resulting matrices onto the images of each hemisphere reveals two main compact regions (top-left, bottom-right), although the matrices do not in themselves provide this spatial information. The resulting clusters are indicated by the coloured bar below the reordered matrices. The number of voxels corresponding to the smaller clusters are shown for each hemisphere (Left = 225, Right = 220). An additional transition area is present between

the main compartments which suggests the possible existence of a third smaller group (cf. green region Fig. 1 D).

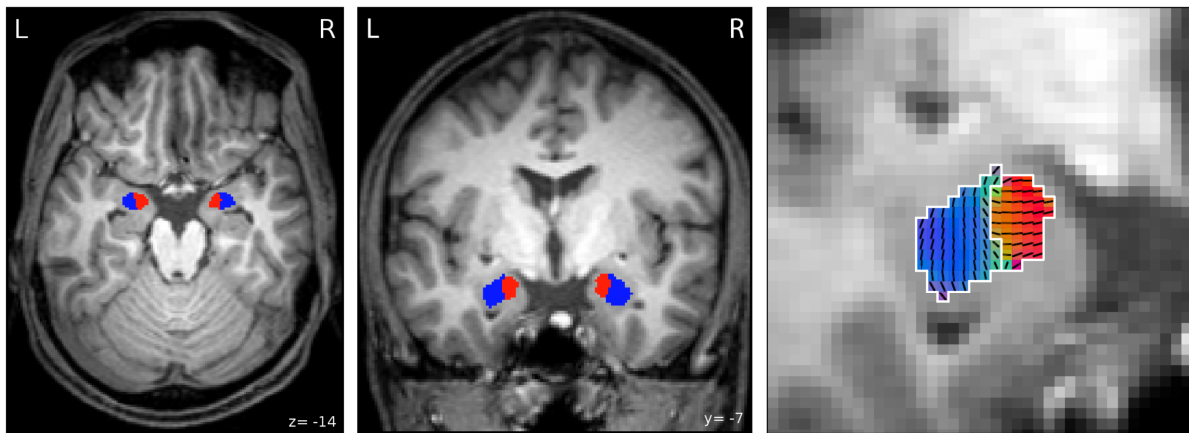


Figure 4. Result of spectral clustering using the averaged similarity matrix. The two main areas are superimposed on a single subject's T1-weighted image (left and middle). The amygdala segments are colour-coded. The medial region is labelled in red and the lateral region in blue. The right panel shows the enlarged left temporal lobe. The averaged diffusion directions are indicated by short lines and superimposed on the amygdala. The colour also represents the diffusion orientation. The white lines correspond to the boundaries computed by the clustering algorithm.

Probabilistic Map of the Amygdala Based on Directions of Maximum Diffusion

The probabilistic map found using this method of amygdala parcellation characterizes the inter-subject variability. It was created by clustering the individual DTI data, followed by spatial normalization and averaging across subjects, and shows good agreement with clustering of the averaged DTI data (Fig. 5). We also computed the distribution of the centroids of each cluster across subjects. This revealed a similarity of localization of the clusters (Fig. 6). In all subjects, the FA values found in the amygdala were much lower than in the white matter. The mean FA values and standard deviation for the lateral subdivision were 0.128 ± 0.024 and for the medial region 0.116 ± 0.024 , with no remarkable differences between both hemispheres.

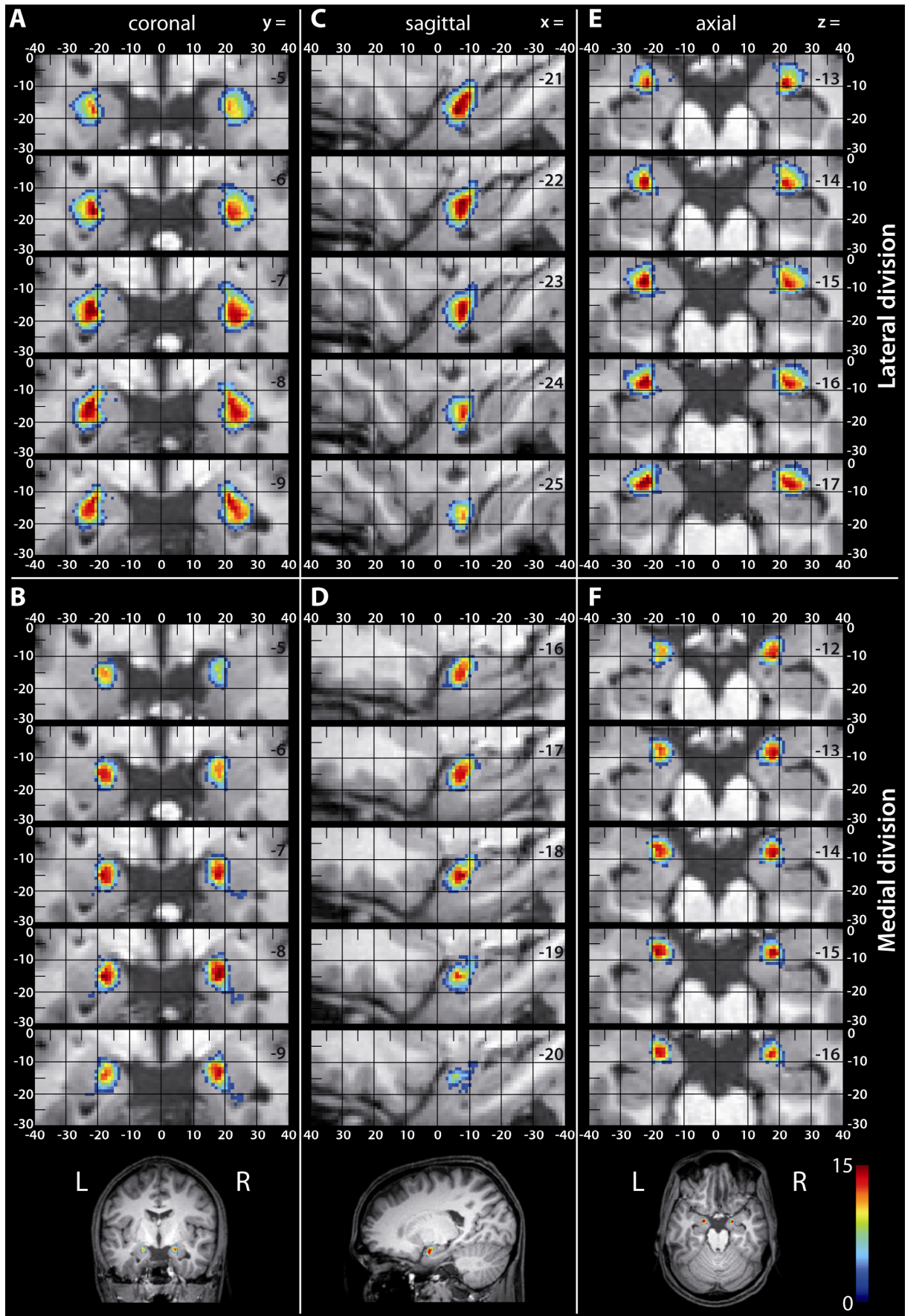


Figure 5. Probabilistic maps of amygdala data. The two amygdaloid subregions derived from individually clustered DTI maps (15 subjects) are superimposed on the structural T1 image of one subject. Left column, coronal sections; middle column, sagittal sections of the left amygdala; right column, axial sections. Maps of the lateral (A, C, E) and medial (B, D, F) cluster across several sections.

Coordinates are in Talairach space. The overlap of the regions from all subjects is colour-coded using the indicated colour map with a minimum overlap of two subjects. An overlap of all 15 subjects is labelled in red. A volumetric reading (grid system) assist to a better localization.

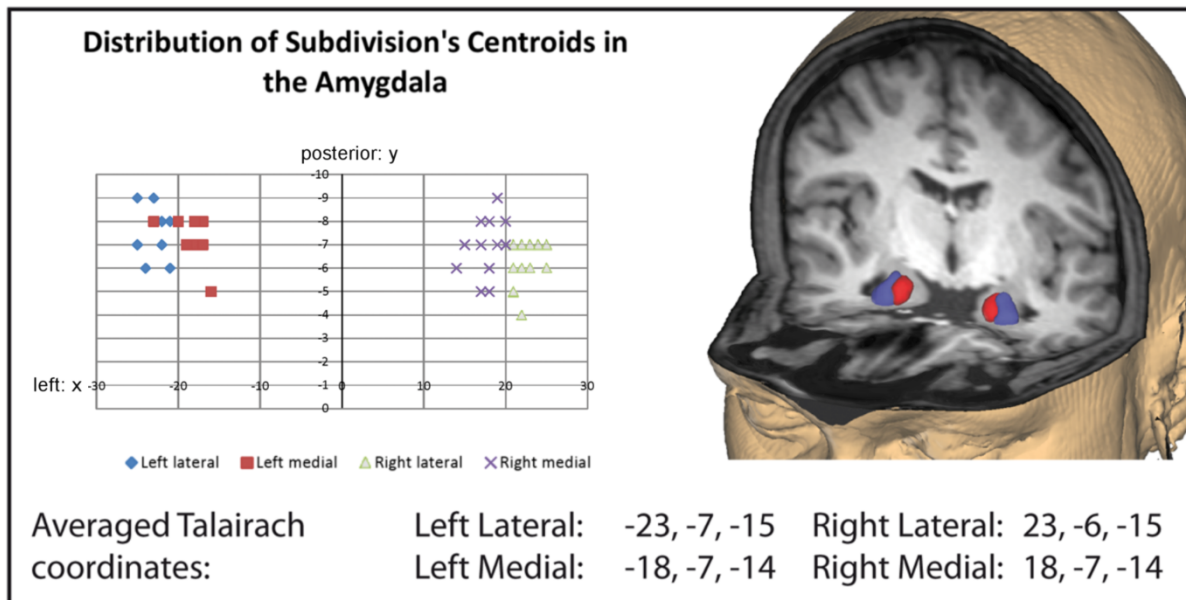


Figure 6. Centroid distribution. (Left) Location of the computed centroids of each subject's subregions. Left and right side of the chart indicate cerebral hemispheres. Vertical axis corresponds to the postero-anterior axis. Coordinates are averaged and given in Talairach space. (Right) 3-D reconstruction of the probabilistic amygdaloid subregions superimposed on a single subject's T1-weighted image.

Discussion

This non-invasive method for subdividing the amygdala may allow structure and function to be directly correlated within the same living human subjects (cf. Johansen- Berg et al. 2005).

It is instructive to compare these maps with careful microscopic examination of sections through the amygdala of a human cadaver brain (Fig. 2). The thickness of the brain section is 30 μm , and its in-plane resolution is only 2 μm , while the MR image resolution is (1.7 mm)³ (cf. box in Fig. 2). The bundles of myelinated fibres are not resolved in the lower resolution MR images, and a significant partial voluming effect is apparent. These bundles may contribute to the main orientations found using DTI. The spatial resolution of the DTI data does not allow discrimination of finer scale structures in the amygdala, but apparently it can distinguish the lateral group of nuclei from the medial nuclear complex.

The precise relationship of the clusters we have found with the known amygdaloid nuclei remains, however, a topic for further investigation. The main orientations appear to correspond to amygdalar connectivity pathways documented in animal brains. Figures 1 and 4 show the blue component labeling the dorso-ventral orientation. Experimental findings describe a well established connection between the lateral amygdala and somatosensory cortical areas (Shi and Cassell 1998; Pikkarainen and Pitkänen 2001; Grossman et al. 2008). The latero-medial direction is labeled in red. Tract tracing studies have reported that the medial part of the amygdala performs an essential role in intra-amygdaloid connections, as well as forming the main output source of the amygdaloid complex (Jolkkonen and Pitkänen 1998; Cassell et al. 1999; Fudge and Tucker 2009). The green-coded group of voxels has a generally anterior-posterior orientation. This region is relatively compact. Fiedler graph analysis reveals a transition area, which could perhaps also be considered as a subdivision (de Olmos 2004). However, due to the inter-subject size variability and the lower coherence

values given by Cramer's V, we are reluctant to include this as a separate subregion, and it will be the object of future investigation.

Fibrearchitectonic preparations (de Olmos 2004) reveal that the lateral and basolateral nuclei are characterized by numerous small fibre bundles running diagonally in a dorsolateral-to-ventromedial direction – a potential microanatomical substrate for the blue cluster found in the DTI data. In the medial nuclear complex (medial, anterior cortical, and ventral cortical nuclei) fibres have a tendency to run in a transverse direction – a possible correlate for the red cluster. The intermediate group of nuclei (central and basomedial nuclei) could be the microstructural substrate of the green cluster.

The probabilistic atlas provided by cytoarchitectonic studies has been increasingly used as a guide for in vivo studies of areas within the amygdala. Indeed, this methodology constitutes the first classification tool for a better understanding of the amygdala. However, the resolution used at MR standard field strength (≤ 3 Tesla) is generally no better than 3 mm isotropic for functional studies, and 1 mm isotropic for structural images. Given the fine detail of the amygdala just discussed, significant partial-volume effects are likely. This in vivo segmentation of the amygdala based on DTI data can thus present similar problems. However, the study presented may assist identification of the amygdaloid subregions for MR images at standard field strength.

Future enhancements may also improve amygdala parcellation. A greater number of radio frequency (RF) receive coil channels can increase the signal to noise ratio, allowing smaller voxels to be used. In a pilot study at 3T, DTI was performed with $(1.5 \text{ mm})^3$ resolution using a 32 channel RF coil, but since the amygdala is relatively deep in the brain the SNR improvement was marginal. The higher field strength of 7 T becoming available can give twice the signal-to-noise ratio as well as improved contrast (Triantafyllou, C. et al. 2005), though there are specific problems with DTI due to the relatively long echo times required.

How does diffusion anisotropy arise in grey matter? The diffusion coefficient of water in grey matter is about 2.5 times smaller than in pure water at body temperature, because tissue water diffusion is hindered by cell membranes, intracellular organelles, cytoskeletal structures, and the extracellular glycocalyx (Le Bihan et al. 1995; Le Bihan and Basser 1995). Myelin contributes to diffusion anisotropy, but it is not essential. For instance, anisotropy has been observed in nonmyelinated olfactory nerves (Beaulieu and Allen 1994a; Beaulieu and Allen 1994b). Thalamic fractional anisotropy (FA) values are approximately 0.3. However, there is no significant correlation between myelin water fraction (MWF) and FA (Mädler et al. 2008). Other factors clearly play a role, such as water restriction in the interstitial space between fibres (perpendicular to the axon), cell shape distributions, membrane permeability, and fibre organization (Hille 1971; Vasilescu et al. 1978; Szafer et al. 1995; Andrews et al. 2006). Furthermore, diffusion anisotropy has been shown in unmyelinated neonatal brain tissue (Wimberger et al. 1995).

The data presented here constitute the first MRI evidence for identification in vivo of internal structure within the amygdala, robustly partitioning this important brain region. In this region there is not only tissue anisotropy, but also a characteristic orientation pattern. This investigation has been focused on the non-invasive segmentation in vivo of the human amygdala and the study of diffusion in organized grey matter. Use of this parcellation could form the basis of functional studies with similar resolution of amygdalar-directed structural networks in vivo. This methodology also opens a new way to study morphometry and volumetry of amygdala subdivisions in large groups of living human subjects.

Acknowledgements

The authors would like to thank Demian Wassermann for his advice on the clustering problem, Timm Wetzels for providing the diffusion-weighted MR datasets, Enrico Kaden for pre-processing the diffusion-weighted images, Christian Labadie for his useful advice and

discussions about diffusion in grey matter, Heike Schmidt-Duderstedt for her assistance in preparing the graphics and the anonymous reviewers for their helpful comments and advice regarding this manuscript.

The authors declare no conflict of interest.

References

- Aggleton J.P., 1992. *The Amygdala: Neurobiological Aspects of Emotion, Memory, and Mental Dysfunction*. New York: Wiley-Liss.
- Alheid G.F., Heimer L., 1988. New perspectives in basal forebrain organization of special relevance for neuropsychiatric disorders: The striatopallidal, amygdaloid, and corticopetal components of substantia innominata. *Neuroscience*. 27:1-39.
- Amaral D.G., Price J.L., Pitkänen A., Carmichael S.T., 1992. Anatomical organization of the primate amygdaloid complex. In: Aggleton J.P., (Ed.), *The Amygdala: Neurobiological Aspects of Emotion, Memory, and Mental Dysfunction*. New York: Wiley-Liss. p 1-66.
- Amunts K., Kedo O., Kindler M., Pieperhoff P., Mohlberg H., Shah N.J., Habel U., Schneider F., Zilles K., 2005. Cytoarchitectonic mapping of the human amygdala, hippocampal region and entorhinal cortex: Intersubject variability and probability maps. *Anat Embryol*. 210:343-352.
- Andrews T.J., Osborne M.T., Does M.D., 2006. Diffusion of myelin water. *Magn Reson Med*. 56:381-385.
- Anwander A., Tittgemeyer M., von Cramon D.Y., Friederici A.D., Knösche T.R., 2007. Connectivity-based parcellation of Broca's area. *Cereb Cortex*. 17:816-825.
- Assaf Y., Pasternak O., 2008. Diffusion tensor imaging (DTI)-based white matter mapping in brain research: A review. *J Mol Neurosci*. 34:51-61.
- Basser P.J., 1993. Cable equation for a myelinated axon derived from its microstructure. *Med Biol Eng Comput*. 31:S87-S92.

- Beaulieu C., Allen P.S., 1994a. Determinants of anisotropic water diffusion in nerves. *Magn Reson Med.* 31:394-400.
- Beaulieu C., Allen P.S., 1994b. Water diffusion in the giant axon of the squid: Implications for diffusion-weighted MRI of the nervous system. *Magn Reson Med.* 32:579-583.
- Beckmann M., Johansen-Berg H., Rushworth M.F.S., 2009. Connectivity-based parcellation of human cingulate cortex and its relation to functional specialization. *J Neurosci.* 29:1175-1190.
- Behrens T.E.J., Johansen-Berg H., Woolrich M.W., Smith S.M., Wheeler-Kingshott C.A.M., Boulby P.A., Barker G.J., Sillery E.L., Sheehan K., Ciccarelli O., Thompson A.J., Brady J.M., Matthews P.M., 2003. Non-invasive mapping of connections between human thalamus and cortex using diffusion imaging. *Nature Neurosci.* 6:750-757.
- Brockhaus H., 1938. Zur normalen und pathologischen Anatomie des Mandelkerngebietes. *J Psychol Neurol.* 49:1-136.
- Cassell M.D., Freedman L.J., Shi C., 1999. The intrinsic organization of the central extended amygdala. *Ann N Y Acad Sci.* 877:217-241.
- Cramer, H., 1946. *Mathematical Methods of Statistics.* Princeton University Press, Princeton, NJ.
- de Olmos J.S., 2004. Amygdala. In: Paxinos G., Mai J.K., (Eds.), *The Human Nervous System (2nd Ed.)*. San Diego: Elsevier Academic Press. p 739-868.
- Devlin J.T., Sillery E.L., Hall D.A., Hobden P., Behrens T.E.J., Nunes R.G., Clare S., Matthews P.M., Moore D.R., Johansen-Berg H., 2006. Reliable identification of the auditory thalamus using multi-modal structural analyses. *Neuroimage.* 30:1112-1120.
- Douek P., Turner R., Pekar J., Patronas N., Le Bihan D., 1991. MR color mapping of myelin fiber orientation. *J Comput Assist Tomogr.* 15:923-929.

- Draganski B., Kherif F., Klöppel S., Cook P.A., Alexander D.C., Parker G.J.M., Deichmann R., Ashburner J., Frackowiak R.S.J., 2008. Evidence for segregated and integrative connectivity patterns in the human basal ganglia. *J Neurosci.* 28:7143-7152.
- Duvernoy H.M., 1999. *The Human Brain. Surface, Blood Supply, and Three-Dimensional Sectional Anatomy.* Wien: Springer.
- Fudge J.L., Tucker T., 2009. Amygdala projections to central amygdaloid nucleus subdivisions and transition zones in the primate. *Neuroscience.* 159:819-841.
- Gallyas F., 1979. Silver staining of myelin by means of physical development. *Neurol Res.* 1:203-209.
- Grossman S.E., Fontanini A., Wieskopf J.S., Katz D.B., 2008. Learning-related plasticity of temporal coding in simultaneously recorded amygdala-cortical ensembles. *J Neurosci.* 28:2864-2873.
- Heimer L., Harlan R.E., Alheid G.F., Garcia M.M., de Olmos J., 1997. Substantia innominata: A notion which impedes clinical-anatomical correlations in neuropsychiatric disorders. *Neuroscience.* 76:957-1006.
- Higham D.J., Kalna G., Kibble M., 2007. Spectral clustering and its use in bioinformatics. *J Comput Appl Math.* 204:25-37.
- Hille B., 1971. The hydration of sodium ions crossing the nerve membrane. *Proc Natl Acad Sci USA.* 68:280-282.
- Horinek D., Varjassyova A., Hort J., 2007. Magnetic resonance analysis of amygdalar volume in Alzheimer's disease. *Curr Opin Psychiatry.* 20:273-277.
- Jaermann T., De Zanche N., Staempfli P., Pruessmann K.P., Valavanis A., Boesiger P., Kollias S.S., 2008. Preliminary experience with visualization of intracortical fibers by focused high-resolution diffusion tensor imaging. *Amer J Neuroradiol.* 29:146-150.

- Jellison B.J., Field A.S., Medow J., Lazar M., Salamat M.S., Alexander A.L., 2004. Diffusion tensor imaging of cerebral white matter: A pictorial review of physics, fiber tract anatomy, and tumor imaging patterns. *Amer J Neuroradiol.* 25:356-369.
- Jenkinson M., Bannister P., Brady M., Smith S., 2002. Improved optimization for the robust and accurate linear registration and motion correction of brain images. *Neuroimage.* 17:825-841.
- Johansen-Berg H., Behrens T.E.J., Robson M.D., Drobnjak I., Rushworth M.F.S, Brady J.M., Smith S.M., Higham D.J., Matthews P.M.. 2004. Changes in connectivity profiles define functionally distinct regions in human medial frontal cortex. *Proc Natl Acad Sci USA.* 101:13335-13340.
- Johansen-Berg H., Behrens T.E.J., Sillery E., Ciccarelli O., Thompson A.J., Smith S.M., Matthews P.M., 2005. Functional-anatomical validation and individual variation of diffusion tractography-based segmentation of the human thalamus. *Cereb Cortex.* 15:31-39.
- Jolkkonen E., Pitkänen A., 1998. Intrinsic connections of the rat amygdaloid complex: Projections originating in the central nucleus. *J Comp Neurol.* 395:53-72.
- Klein J.C., Behrens T.E.J., Robson M.D., Mackay C.E., Higham D.J., Johansen-Berg H., 2007. Connectivity-based parcellation of human cortex using diffusion MRI: Establishing reproducibility, validity and observer independence in BA 44/45 and SMA/pre-SMA. *Neuroimage.* 34:204-211.
- Lawes I.N.C., Barrick T.R., Murugam V., Spierings N., Evans D.R., Song M., Clark C.A., 2008. Atlas-based segmentation of white matter tracts of the human brain using diffusion tensor tractography and comparison with classical dissection. *Neuroimage.* 39:62-79.

- Le Bihan D., Basser P.J. 1995. Molecular diffusion and nuclear magnetic resonance. In: Le Bihan D., (Ed.), *Diffusion and Perfusion Magnetic Resonance Imaging*. New York: Raven Press. pp. 5-17.
- Le Bihan D., Turner R., Patronas N., 1995. Diffusion MR imaging in normal brain and in brain tumors. In: Le Bihan D., (Ed.), *Diffusion and Perfusion Magnetic Resonance Imaging*. New York: Raven Press. pp. 134-140.
- Mädler B., Drabycz S.A., Kolind S.H., Whittall K.P., MacKay A.L., 2008. Is diffusion anisotropy an accurate monitor of myelination? Correlation of multicomponent T2 relaxation and diffusion tensor anisotropy in human brain. *Magn Reson Imaging*. 26:874-888.
- Mai J.K., Paxinos G., Voss T. 2008. *Atlas of the Human Brain (3rd Ed.)*. New York: Academic Press.
- McDonald A.J., 1992. Cell types and intrinsic connections of the amygdala. In: Aggleton J.P., (Ed.), *The Amygdala: Neurobiological Aspects of Emotion, Memory, and Mental Dysfunction*. New York: Wiley-Liss. pp. 67-96.
- Mori S., Oishi K., Jiang H., Jiang L., Li X., Akhter K., Hua K., Faria A.V., Mahmood A., Woods R., Toga A.W., Pike G.B., Neto P.R., Evans A., Zhang J., Huang H., Miller M.I., van Zijl P., Mazziotta J., 2008. Stereotaxic white matter atlas based on diffusion tensor imaging in an ICBM template. *Neuroimage*. 40:570-582.
- Mori S., Wakana S., Nagae-Poetscher L.M., van Zijl P.C.M., 2005. *MRI Atlas of Human White Matter*. Amsterdam: Elsevier.
- Ng A.Y., Jordan M.I., Weiss Y., 2002. On spectral clustering: Analysis and an algorithm. *Proc Neur Inform Proc Syst (NIPS)*. 14:849-856.
- Nieuwenhuys R., Voogd J., van Huijzen C., 2008. *The Human Central Nervous System (4th Ed.)*. Berlin: Springer.

- Nucifora P.G.P., Verma R., Lee S.K., Melhem E.R., 2007. Diffusion-tensor MR imaging and tractography: Exploring brain microstructure and connectivity. *Radiology*. 245:367-384.
- Oishi K., Zilles K., Amunts K., Faria A., Jiang H., Li X., Akhter K., Hua K., Woods R., Toga A.W., Pike G.B., Rosa-Neto P., Evans A., Zhang J., Huang H., Miller M.I., van Zijl P.C.M., Mazziotta J., Mori S., 2008. Human brain white matter atlas: Identification and assignment of common anatomical structures in superficial white matter. *Neuroimage*. 43:447-457.
- Pikkarainen M., Pitkänen A., 2001. Projections from the lateral, basal and accessory basal nuclei of the amygdala to the perirhinal and postrhinal cortices in rat. *Cereb Cortex*. 11:1064-1082.
- Reese T.G., Heid O., Weisskoff R.M., Wedeen V.J. 2003. Reduction of eddy-current-induced distortion in diffusion MRI using a twice-refocused spin echo. *Magn Reson Med*. 49:177-182.
- Schirmer A., Escoffier N., Zysset S., Koester D., Striano T., Friederici A.D., 2008. When vocal processing gets emotional: on the role of social orientation in relevance detection by the human amygdala. *Neuroimage*. 40:1402-1410.
- Shi C.J., Cassell M.D., 1998. Cascade projections from somatosensory cortex to the rat basolateral amygdala via the parietal insular cortex. *J Comp Neurol*. 399:469-491.
- Szafer A., Zhong J., Gore J.C., 1995. Theoretical model for water diffusion in tissues. *Magn Reson Med*. 33:697-712.
- Talairach J., Tournoux P., 1988. *Co-Planar Stereotaxic Atlas of the Human Brain. 3-Dimensional Proportional System: An Approach to Cerebral Imaging*. Stuttgart: Thieme.
- Thirion J.P., 1998. Image matching as a diffusion process: An analogy with Maxwell's demons. *Med Image Anal*. 2:243-260.

- Tomassini V., Jbabdi S., Klein J.C., Behrens T.E.J., Pozzilli C., Matthews P.M., Rushworth M.F.S., Johansen-Berg H., 2007. Diffusion-weighted imaging tractography-based parcellation of the human lateral premotor cortex identifies dorsal and ventral subregions with anatomical and functional specializations. *J Neurosci.* 27:10259-10269.
- Triantafyllou C., Hoge R.D., Krueger G., Wiggins C.J., Potthast A., Wiggins G.C., Wald L.L., 2005. Comparison of physiological noise at 1.5 T, 3 T and 7 T and optimization of fMRI acquisition parameters. *Neuroimage.* 26:243-250.
- Turner R., Le Bihan D., Chesnick A.S., 1991. Echo-planar imaging of diffusion and perfusion. *Magn Reson Med.* 19:247-253.
- Van Hecke W., Sijbers J., D'Agostino E., Maes F., De Backer S., Vandervliet E., Parizel P.M., Leemans A., 2008. On the construction of an inter-subject diffusion tensor magnetic resonance atlas of the healthy human brain. *Neuroimage.* 43:69-80.
- Vasilescu V., Katona E., Simplaceanu V., Demco D., 1978. Water compartments in the myelinated nerve. III. Pulsed NMR results. *Experientia.* 34:1443-1444.
- Wakana S., Jiang H., Nagae-Poetscher L.M., van Zijl P.C.M., Mori S., 2004. Fiber tract-based atlas of human white matter anatomy. *Radiology.* 230:77-87.
- Weiskopf N., Hutton C., Josephs O., Turner R., Deichmann R., 2007. Optimized EPI for fMRI studies of the orbitofrontal cortex: Compensation of susceptibility-induced gradients in the readout direction. *MAGMA.* 20:39-49.
- Wiegell M.R., Tuch D.S., Larsson H.B.W., Wedeen V.J., 2003. Automatic segmentation of thalamic nuclei from diffusion tensor magnetic resonance imaging. *Neuroimage.* 19:391-401.
- Wimberger D.M., Roberts T.P., Barkovich A.J., Prayer L.M., Moseley M.E., Kucharczyk J., 1995. Identification of "premyelination" by diffusion-weighted MRI. *J Comput Assist Tomogr.* 19:28-33.